Bifurcation analysis of optically induced dynamics in nematic liquid crystals: circular polarization at normal incidence

E. Brasselet, T. V. Galstian,* and L. J. Dubé†

Département de Physique, de Génie Physique, et d'Optique, Université Laval, Cité Universitaire, Québec, Canada G1K7P4

D. O. Krimer and L. Kramer‡

Physikalisches Institut der Universität Bayreuth, D-95440 Bayreuth, Germany

Received December 10, 2004; revised manuscript received February 15, 2005; accepted February 28, 2005

We present a detailed bifurcation analysis of the nonlinear reorientation dynamics of a homeotropically aligned nematic liquid-crystal film excited by a circularly polarized beam at normal incidence with the light intensity as the control parameter. The secondary bifurcation above the optical Fréedericksz transition threshold is identified as a supercritical Hopf bifurcation leading to quasi-periodicity, and the subsequent discontinuous transition from quasi-periodicity to periodicity at higher intensity is identified as a homoclinic bifurcation. The bifurcation scenario is compared with the one obtained in the case of an ordinary light wave at small oblique incidence. Despite an analogous sequence of transitions, there are substantial differences. © 2005 Optical Society of America

OCIS codes: 190.0190, 160.3710.

1. INTRODUCTION

Over the past two decades the effects associated with the propagation of laser light in a liquid crystal (LC) have been studied intensively.[1–4] The long-range orientational order of the molecules in these media adds a collective character to the light–matter interaction and generates a unique spatiotemporal feedback mechanism responsible for the rich dynamics of the optically induced orientational phenomena reported thus far.[5–11] A further attractive feature of these systems is that a rigorous theoretical framework [at least for nematic liquid crystals[12] (NLCs)] is available, involving Maxwell's equations together with the hydrodynamic equations of the LC. The description involves primarily the dynamics of the director **n**, a unit vector that designates the local axis of average orientation of the molecules.

Among the different light–LC interaction geometries, the case of a circularly polarized beam impinging normally on a homeotropic NLC film (i.e., the molecules are perpendicular to the cell substrates) has received much attention ever since the discovery of the optical Fréedericksz transition (OFT) by Zolot'ko *et al.* in 1981.[13] In 1986, Santamato *et al.*[14] realized that the changes in the polarization of light, as it passes through the reoriented optically anisotropic NLC, are associated with spin-angular-momentum transfer from light to matter. In that case, a collective rotation of the NLC molecules was observed that allowed the experimental identification of the OFT as a subcritical Hopf bifurcation. The theoretical description of this bifurcation was done by Zolot'ko *et al.* in 1990,[15] pointing out the importance of nonadiabatic LC distortions related to twist deformations of the director. Marrucci *et al.*,[16] in 1992, extended investigations to high excitation intensities and high reorientation amplitude. They observed an unexpected discontinuous transition with large hysteresis from a precession regime with small reorientation amplitude to one with large reorientation. Some years later, a qualitative mechanism based on nonuniform spin-angular-momentum deposition from the light to the NLC was introduced to explain the origin of such a transition.[17] More recently, some of the present authors identified an additional continuous secondary instability between the OFT and the abrupt transition,[18] and a preliminary description of the bifurcation scenario in the limit of the infinite-plane-wave approximation was reported in Ref. 19; however, neither the exact description of uniform precession (UP) limit cycles nor the determination of the unstable limit cycles was possible with this model, and thus the capture of all the finer details of the dynamics was not possible. Finally, experimental investigations have recently been devoted to identify the role of a finite beam size, which has been shown in realistic situations to play an important role in the reorientation dynamics.[20] Despite these cumulative advances, it is fair to say that a complete theoretical formulation is still lacking.

Although it is clear that a full understanding of the experimental observations of the light-induced reorientation dynamics of NLC films must take into account the finite size of the incident beam, progress may be achieved if one sets out to establish firmly the exact nature of the bifurcation scenario in the infinite-plane-wave situation. The resulting calculations can then serve as a guide for further improvements toward a description of the finite

 © 2005 Optical Society of America

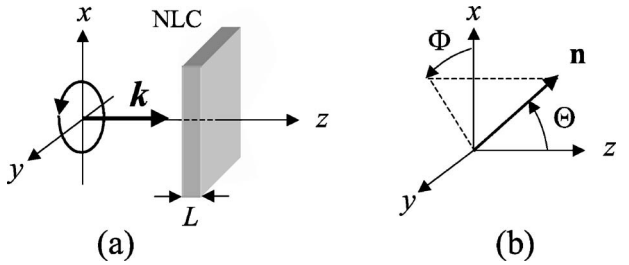

Fig. 1. (a) Interaction geometry in the Cartesian coordinate system (x,y,z), where $\mathbf{k}$ is the wave vector of the circularly polarized excitation light, NLC is the nematic liquid-crystal film, and L is the cell thickness. (b) Representation of the director $\mathbf{n}=(\sin\Theta\cos\Phi,\sin\Theta\sin\Phi,\cos\Theta)$ in terms of the standard spherical angles Θ and Φ.

beam case. To obtain such standard results is the main purpose of our contribution. Alternatively, our theoretical results may invite new experimental studies with a wider range of beam aspect ratios. Besides the infinite-plane-wave idealization, the only relevant approximation is the neglect of dynamical flow in the LC. On the numerical side, we use a reorientation modal expansion whose accuracy and convergence properties are easily controlled by the number of modes included in the calculation.

In this paper we present the detailed analysis of the bifurcation scenario in the case of a circularly polarized excitation at normal incidence by describing the director with the usual spherical angles (Θ,Φ). This allows the exact determination of all the UP states (stable and unstable). It is shown that the secondary instability above the optical Fréedericksz transition threshold is a supercritical Hopf bifurcation. As a result of this bifurcation, a quasi-periodic dynamics is generated in which the motion of the director is a combination of precession and nutation with distinct fundamental frequencies. Moreover, the following discontinuous transition from the quasi-periodic regime to a UP regime is identified as a homoclinic bifurcation.[21–23] These results are compared with experiments with the help of a pair of observables that allows one to distinguish nutation from precession. Finally, the present situation of a circularly polarized excitation at normal incidence is compared with the case of an ordinary light wave at small oblique incidence, which also possesses an analogous sequence of a secondary Hopf bifurcation followed by a homoclinic bifurcation.

The paper is organized as follows. Section 2 presents the theoretical bifurcation scenario and its comparison with experiment. In Section 3, the linear stability analysis of the UP states is performed, and the nature of the successive bifurcations is identified and discussed. Finally, our conclusions and perspectives are summarized in Section 4.

2. DYNAMICAL SCENARIO

A. Theoretical Model

We choose a Cartesian coordinate system (x,y,z) with the z axis along the direction of the wave vector $\mathbf{k}$ of light [Fig. 1(a)]. The calculations are developed in the infinite-plane-wave approximation, justified if the spot size of the excitation beam is significantly larger than the thickness L of the NLC film. Under this assumption, all the relevant functions depend solely on the spatial coordinate z and the time t. In this case, the director representation $\mathbf{n}=(\sin\Theta\cos\Phi,\sin\Theta\sin\Phi,\cos\Theta)$ [Fig. 1(b)], together with the homeotropic boundary conditions $[\Theta(0,t)=\Theta(L,t)=0$ and $\partial_z\Phi(0,t)=\partial_z\Phi(L,t)=0]$, suggests the expansion of angles Θ and Φ in an appropriate set of orthogonal functions[24]:

$$\Theta(z,t) = \sum_{n=1}^{\infty} \Theta_n(t)\sin(n\pi z/L), \tag{1}$$

$$\Phi(z,t) = \Phi_0(t) + \sum_{n=1}^{\infty} \Phi_n(t)\frac{\sin[(n+1)\pi z/L]}{\sin(\pi z/L)}. \tag{2}$$

The mode $\Phi_0(t)$ does not depend on z and describes the pure rotation of the director around the z axis. The dynamical equations of motion for angles Θ and Φ are obtained from the balance between the torques (elastic, electromagnetic, and viscous) acting on the NLC. These individual torques are calculated from the variational derivatives of the elastic and the electromagnetic free-energy densities and the dissipation function density, respectively.[25] Equations (A1) in Appendix A correspond to the situation in which the velocity field is neglected. The equations for each amplitude Θ_n and Φ_n are then obtained by projecting Eqs. (A1) on each mode to produce an infinite-dimensional integrodifferential problem [Eqs. (A7)]. The ensuing numerics are made tractable by a reduction to a finite-dimensional system by using a truncated model expansion for the angles: $(\Theta_1,\ldots,\Theta_N;\Phi_0,\Phi_1,\ldots,\Phi_M)$. Finally, the resulting set of $N+M+1$ time-dependent Eqs. (A7) is solved simulta-

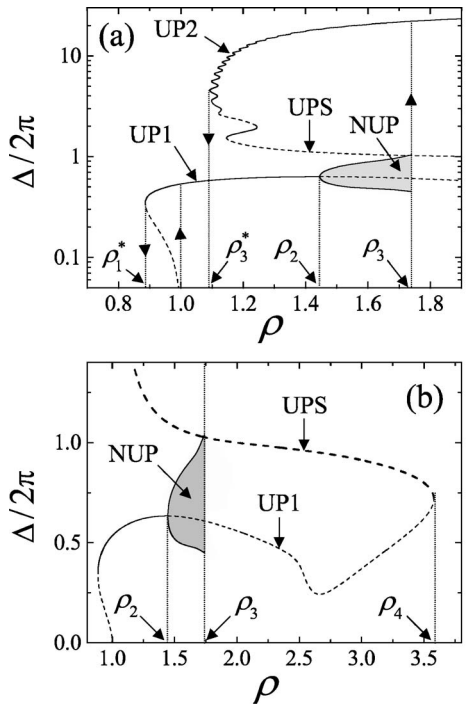

Fig. 2. (a) $\Delta/2\pi$ on a log scale versus ρ for $\rho<2$ and $\Delta<50\pi$. (b) $\Delta/2\pi$ on a linear scale versus ρ for $\rho<4$ and $\Delta<3\pi$. Solid (dashed) curves correspond to stable (unstable) solutions.

Table 1. Calculated Values of the Thresholds ρ_2 and ρ_3 versus the Number of Modes N and M Retained in the Modal Expansion Defined in the Text

	Transition Threshold ρ_2						Transition Threshold ρ_3					
	N Mode						N Mode					
M Mode	1	2	3	4	5	6	1	2	3	4	5	6
1	—	—	—	—	—	—	—	—	—	—	—	—
2	—	—	—	—	—	—	—	—	—	—	—	—
3	1.66	—	1.46	1.46	1.45	1.45	2.07	—	1.76	1.78	1.77	1.77
4	1.63	—	1.45	1.45	1.45	1.45	2.07	—	1.75	1.79	1.77	1.77
5	1.63	—	1.45	1.45	1.45	1.45	2.02	—	1.74	1.77	1.75	1.75
6	1.63	—	1.45	1.45	1.45	1.45	2.01	—	1.74	1.77	1.75	1.75

neously with Eqs. (A4) governing the optical fields.

For the present calculations, we use the material parameters corresponding to the nematic E7 used in the experiments: The splay, twist, and bend elastic constants of the NLC are taken to be $K_1=11.09\times10^{-12}$ N, $K_2=5.82\times10^{-12}$ N, $K_3=15.97\times10^{-12}$ N; the refractive indices of the extraordinary light and ordinary light are taken to be $n_E=1.746$, $n_o=1.522$[26]; $\lambda=532$ nm (wavelength of the laser); and $\gamma_1/K_3=10^{10}$ s m^{-2},[27] where γ_1 is the rotational viscosity. The thickness of the NLC film is taken to be $L=100$ μm. We also introduce for convenience a characteristic time $\tau_{\mathrm{NLC}}=\gamma_1 L^2/\pi^2 K_3$ (typically, for $L=100$ μm, $\tau_{\mathrm{NLC}}\simeq 10$ s).

One notes that the coupled equations for both the director and the optical field [Eqs. (A1), (A4), and (A7)], together with the boundary conditions given by Eqs. (A8) and (A10), are explicitly invariant with respect to rotations around the z axis, namely, to the change $\Phi\rightarrow\Phi+\delta\Phi$ as a consequence of isotropy in the (x,y) plane. As a result, the equation for Φ_0 is decoupled from the ones for Θ_n and Φ_n ($n\geqslant 1$). When these modes do not depend on t ($d\Phi_n/dt=d\Theta_n/dt=0$), the angular velocity $d\Phi_0/dt$ has a constant value, and the director precesses uniformly around the z axis (UP state) with a frequency f_0 defined as

$$f_0=\frac{1}{2\pi}\left(\frac{d\Phi_0}{dt}\right)_{\mathrm{UP}}. \tag{3}$$

In this case, the problem is significantly simplified. In fact, instead of solving a system of evolution equations for $\Phi_0(t)$, $\Phi_n(t)$, and $\Theta_n(t)$, we are now faced with a set of nonlinear algebraic equations in Φ_n and Θ_n. After solving these equations numerically and substituting Φ_n and Θ_n into the equation that gives $d\Phi_0(t)/dt$, we can calculate directly the frequency f_0 of the UP.

The preceding comment holds only for circularly polarized light because for an elliptically polarized excitation the rotational invariance is broken. This considerably enriches the dynamics.[28–30]

B. Simulations

The incident light intensity I is taken as the control parameter, and we define $\rho=I/I_F^{\mathrm{CP}}$ as the normalized intensity, where I_F^{CP} is the transition threshold for the OFT under circular polarization excitation (see Appendix A for the explicit expression). To elucidate the importance of the different modes in the actual dynamical behavior, we have calculated the bifurcation scenario for different combinations of spatial mode expansion (N,M). We introduce the phase delay $\Delta(t)$ defined as (see Appendix A)

$$\Delta(t)=\frac{2\pi}{\lambda}\int_0^L [n_e(z,t)-n_o]dz. \tag{4}$$

This phase has an experimental counterpart in that the quantity $\Delta/2\pi$ roughly represents the number of self-diffraction rings in the far field.[31] Also the UP states are characterized by a time-independent phase delay, $\Delta=$const., whereas $d\Delta/dt\neq 0$ for nonuniform precession (NUP) states.

Increasing the number of modes leads to convergence of the system's behavior toward the one presented in Fig. 2 in which the phase delay $\Delta/2\pi$ is plotted versus the normalized intensity ρ. The solid curves represent stable UP states, and the dashed curves correspond to unstable UP states (see Subsection 3.A for the linear stability analysis of the UP states). The region in gray corresponds to a NUP regime ($d\Delta/dt\neq 0$) in which nutation is coupled to precession. In this regime, the lower and the upper curves that define the region in gray correspond to the minimum and the maximum values taken by Δ during its oscillation. The threshold values for the continuous transition at $\rho=\rho_2$, where nutation appears ($\partial_t\Theta\neq 0$), and for the discontinuous transition at $\rho=\rho_3$, where the system abruptly bifurcates toward a large reorientation regime ($\Theta\sim 1$), are summarized in Table 1 for different pairs (N,M). We can see that the values for ρ_2 and ρ_3 converge toward common values for large enough values of N and M; an empty entry indicates that the bifurcation scenario for the corresponding (N,M) follows a different sequence of transitions.

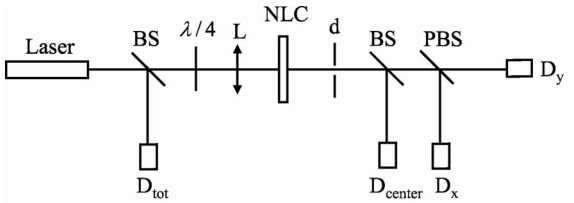

Fig. 3. Experimental setup. Laser: Verdi laser (from Coherent) operating at 532 nm; BS, beam splitter; $\lambda/4$, quarter-wave plate; L, lens; d, diaphragm; PBS, polarizing beam splitter; D_i, photodetectors.

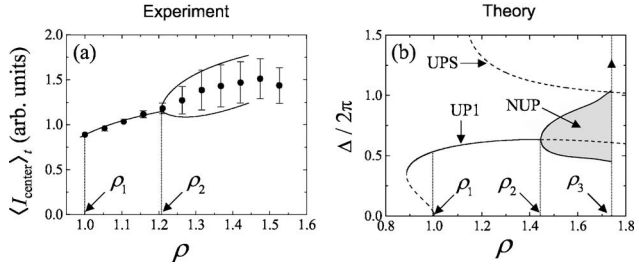

Fig. 4. (a) Experimental $\langle I_{\text{center}}(\rho)\rangle_t$ (filled circles). The vertical bars are the standard deviation of $I_{\text{center}}(t)$ for the corresponding value of ρ, and the solid curve is to guide the eye of the extrema of $I_{\text{center}}(t)$. (b) Calculated $\Delta(\rho)$ ($\Delta < 3\pi$).

It appears to be enough to retain only a few modes for the angles (Θ,Φ) to describe accurately the sequence of bifurcations. Because an absolute precision of 0.01 both for ρ_2 and for ρ_3 is achieved when $N,M \geqslant 6$, we decided to perform all further calculations appearing here with $N=M=6$.

By definition, the OFT occurs at $\rho=1$, where we observe that the system settles to a UP state with a small reorientation amplitude ($\Delta \sim \pi$ or, equivalently, $\Theta^2 \ll 1$) labeled UP1 [Fig. 2(a)] (see Ref. 32 for details concerning the nature of the OFT). When the intensity is decreased from the UP1 regime, the system switches back to the unperturbed state at $\rho=\rho_1^* \simeq 0.88$. When the intensity is increased above the OFT threshold, the UP1 loses its stability at $\rho=\rho_2 \simeq 1.45$, where the NUP regime takes over. Subsequently, the NUP loses stability at $\rho=\rho_3 \simeq 1.75$, where the system abruptly switches to a UP with a large reorientation amplitude ($\Delta \gg 1$ or, equivalently, $\Theta^2 \sim 1$) labeled UP2. When the intensity is decreased in the UP2 regime, the system switches back to the UP1 regime at $\rho=\rho_3^* \simeq 1.09$. Figure 2(b) shows the entire UP1 regime: The unstable branch makes a loop and connects with the other unstable branch, UPS (S for saddle or separatrix; the label will be justified in Section 3), which connects to the UP2 regime. Finally, for $\rho > \rho_4 \simeq 3.58$, one is left with UP2 only.

C. Experiment

We used an experimental apparatus (Fig. 3) that gives simultaneous access to the dynamical behavior related to the polar (Θ) and the azimuthal (Φ) parts of the molecular configuration. This technique is described in more detail in Ref. 20. It consists of a Verdi laser (from Coherent) operating at 532 nm, whose polarization is made circular by using a quarter-wave plate, focused on the NLC cell with a lens of focal length $f=150$ mm. The beam diameter is $2w_0=30$ μm at the sample location, and the cell thickness is $L=75$ μm. The director dynamics is retrieved by the analysis of the central part of the emerging beam after the diaphragm d. Photodiodes D_{center}, D_x, and D_y collect, respectively, the total intensity of the central part of the beam, I_{center}, and the intensities, I_x and I_y, of the x and y electric field components ($I_{\text{center}}=I_x+I_y$). The incident intensity I_{tot} is monitored by the photodiode D_{tot}. The data-acquisition frequency is 4 Hz. The behavior of the signal $I_{\text{center}}(t)$ is qualitatively similar to that of $\Delta(t)$, whereas the behavior of the signals $i_x(t) \equiv I_x/I_{\text{center}}$ and $i_y(t) \equiv I_y/I_{\text{center}}$ can be compared with the calculated intensities at the output of the sample, $I_x(t)=|E_x(z=L,t)|^2$ and $I_y(t)=|E_y(z=L,t)|^2$, respectively. In that $i_x(t)=1-i_y(t)$, these time series possess the same dynamical information, and we shall refer to any of these quantities as $i(t)$.

The reorientation amplitude as a function of the incident intensity is experimentally studied by observing $I_{\text{center}}(t)$. Its time-averaged value $\langle I_{\text{center}}\rangle_t$ is plotted in Fig. 4(a) in which the average is performed over a time duration much longer than the precession period $1/f_0$. The vertical bars represent the standard deviation of $I_{\text{center}}(t)$ for a given ρ. We can conclude that an oscillation of the reorientation amplitude of the director takes place above a given intensity $\rho=\rho_2$, corresponding to the appearance of the NUP regime. In Fig. 4(b), the calculated Δ is plotted as a function of ρ. On the other hand, Fig. 5(a) displays the experimental precession frequency f_0 as a function of ρ. This frequency is deduced from the Fourier spectrum of the time series $i(t)$, which exhibits a single frequency $2f_0$ in the UP1 regime. This double frequency arises because the polarization ellipse at the output of the sample is invariant under a rotation of π around the z axis. The transition UP1$\rightarrow$NUP is associated with a sudden change of slope of the precession frequency versus intensity, as predicted by theory [see Fig. 5(b)]. This behavior can be explained as follows. In the NUP regime, the phase shift Δ explores values closer to 2π as ρ increases [see Fig. 4(b)] and the total angular-momentum transfer per photon to the NLC, $(1-\cos\Delta)\hbar$, is correspondingly smaller.

A qualitative agreement between theory and experiment is observed, although the onset of the NUP regime appears at a lower value $\rho_2 \simeq 1.2$ experimental versus $\rho_2 \simeq 1.45$ theoretical), and the precession rate accelerates as ρ increases from 1 to ρ_2 [Fig. 5(a)], whereas a deceleration is predicted by theory [Fig. 5(b)]. Such discrepancies may be attributed to the finite size of the excitation beam, the present aspect ratio being $\delta=2w_0/L=0.4$. For higher values of δ, the deceleration behavior predicted by the infinite-plane-wave theory was in fact observed earlier[16] for $\delta=2$ and $\delta=3$. However, for such large values of δ, the transition UP1$\rightarrow$NUP was not observed. This is probably due to a nonefficient spatial averaging of the light-angular-momentum deposition in the plane (x,y), which is driven by transverse effects. Moreover, $\delta \simeq 2$ has been demonstrated in another context (linearly polarized excitation at normal incidence[34]) to be a critical value for the aspect ratio laser beam. This has led us to choose a smaller beam diameter.

In Section 3, we will relate the transitions UP1 $\rightarrow$NUP and NUP$\rightarrow$UP2 to standard bifurcation scenarios. For this purpose, the linear stability analysis of

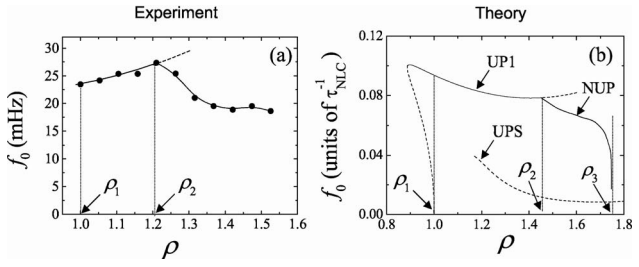

Fig. 5. Precession frequency $f_0(\rho)$. (a) Experiment (filled circles). The solid curve is to guide the eye. (b) Theory.

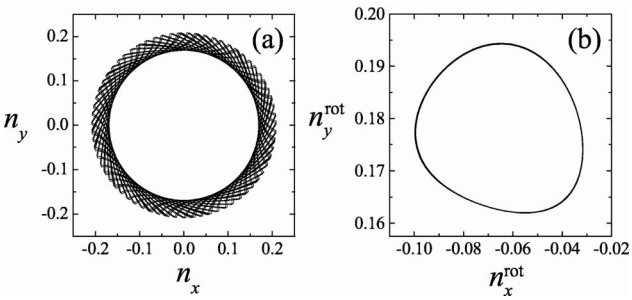

Fig. 6. Director trajectory at $\rho=1.55$. (a) Quasi-periodic behavior in the laboratory frame (n_x,n_y). (b) Periodic limit cycle in the f_0-rotating frame $(n_x^{\rm rot},n_y^{\rm rot})$.

the UP states is first performed, followed by a study of the critical dynamical behavior in the neighborhood of the bifurcations. Finally, the present situation is compared with a closely related interaction geometry that possesses a similar sequence of bifurcations.

3. BIFURCATION ANALYSIS

A. Linear Stability Analysis of Uniform Precession States

The linear stability analysis of the UP states is performed according to the following procedure. We first introduce the vector $\mathbf{x}=(\Theta_1,\ldots,\Theta_N,\Phi_1,\ldots,\Phi_M)$, rewriting Eqs. (A7) as $\dot{\mathbf{x}}=\mathbf{F}(\mathbf{x})$ (the dot denoting the time derivative). The UP states $\mathbf{x}_{\rm UP}$ are then found as solutions of their defining equation $\mathbf{F}(\mathbf{x}_{\rm UP})=0$, and their stability is established by calculating the eigenvalues of the corresponding Jacobian matrix $J_{ij}=(\partial F_i/\partial x_j)_{\mathbf{x}=\mathbf{x}_{\rm UP}}$. For the analysis of the situation depicted in Fig. 2(b) where $\Delta/2\pi<1.4$, it is sufficient to consider the eigenvalue with the largest real part, denoted $\lambda_{\max}$.

We find that the transition at $\rho=\rho_1^*$ is a saddle-node bifurcation. Moreover, the UP1 state represents a stable node ($\lambda_{\max}$ is real and negative) in the hysteretic region within $0.886<\rho<0.911$, changing to a stable focus at $\rho=0.911$, where $\lambda_{\max}$ gives rise to a complex-conjugate pair $\Re(\lambda_{\max})\pm i\Im(\lambda_{\max})$, with $\Re(\lambda_{\max})<0$ and $\Im(\lambda_{\max})\neq 0$. At $\rho=\rho_2$, $\Re(\lambda_{\max})$ crosses zero and becomes positive for larger ρ, indicating a Hopf bifurcation. This transition is supercritical as illustrated in Fig. 2. In Subsection 3.B, we shall see that a limit cycle is born at ρ_2, which corresponds to the appearance of a new frequency f_1 leading to quasi-periodicity.

B. Secondary Supercritical Hopf Bifurcation

One analyzes the dynamical regime arising above the transition threshold $\rho=\rho_2$ by studying the director trajectory. This is illustrated in Fig. 6(a) in which the trajectory in the plane (n_x,n_y) is plotted for $\rho=1.55$ at $z=L/2-\ell$ ($\ell\neq 0$). The reason for this somewhat arbitrary value of z is to have contributions from all polar modes because, by construction, the even modes $\Theta_n\sin(n\pi z/L)$ are zero at the center of the cell ($z=L/2$). The trajectory is not closed in the laboratory frame, indicating quasi-periodicity of the director, i.e., the presence of two incommensurate frequencies f_0 and f_1. In fact, one can isolate the two independent motions, namely, the precession (f_0) and the nutation (f_1) by performing a transformation into a frame that rotates with frequency f_0 around the z axis. The director components $(n_x^{\rm rot},n_y^{\rm rot})$ in this f_0-rotating frame are connected with the components (n_x,n_y) in the laboratory frame by

$$n_x^{\rm rot} = n_y\sin(2\pi f_0 t)+n_x\cos(2\pi f_0 t),$$

$$n_y^{\rm rot} = n_y\cos(2\pi f_0 t)-n_x\sin(2\pi f_0 t). \quad (5)$$

In the rotating frame, the director performs a simple periodic motion with frequency f_1 as is seen in Fig. 6(b).

In the neighborhood of the bifurcation point, the scaling properties of the amplitude $\mathcal{A}$ and the frequency f_1 of the limit cycle born at ρ_2 serve to identify experimentally the nature of the transition as a supercritical Hopf bifurcation. One thus expects to observe the scaling laws $\mathcal{A}(\rho)-\mathcal{A}(\rho_2)=\mathcal{O}(\rho-\rho_2)^{1/2}$ and $f_1(\rho)-f_1(\rho_2)=\mathcal{O}(\rho-\rho_2)$ in the neighborhood of $\rho=\rho_2$. For the purpose of analysis, we define theoretically the amplitude as $\mathcal{A}_{\rm theory}=\max|\mathbf{n}_\perp|-\min|\mathbf{n}_\perp|$, where $|\mathbf{n}_\perp|=(n_x^2+n_y^2)^{1/2}$ is the projection of $\mathbf{n}$ onto the plane of the layer. The experimental observable is chosen to be $\mathcal{A}_{\rm exp}=\mathrm{SD}(I_{\rm center})$, where $\mathrm{SD}(X)$ is the standard deviation of the time series $X(t)$. Clearly, $\mathcal{A}_{\rm theory}$ and $\mathcal{A}_{\rm exp}$ can only be different from zero in the presence of nutation. The results are shown in Fig. 7 in which $\mathcal{A}_{\rm exp}$ is plotted versus ρ (filled circles) and $\mathcal{A}_{\rm theory}$ is shown in the inset (solid curve). The experimental data are fitted by $\mathcal{A}_{\rm exp}(\rho)-\mathcal{A}_{\rm exp}(\rho_2)=\mathcal{O}(\rho-\rho_2)^\gamma$ by using the four points in the range $1.2<\rho<1.4$ and taking $\mathcal{A}_{\rm exp}(\rho_2)$ as the averaged value of $\mathcal{A}_{\rm exp}$ for $\rho<1.2$. We find $\gamma=0.46\pm0.08$ (dashed curve) and $\rho_2=1.208\pm0.001$. A similar fit to the theoretical values leads to $\gamma=1/2$ (dashed curve in the inset of Fig. 7). One recalls that the limits of the applicability of the scaling laws around the bifurcation point is restricted to intensity values that are not too far above ρ_2. This allows us to understand the deviation of both the theoretical calculations and the experimental data from the square-root behavior. As to the frequency f_1, the linear scaling law is also well verified experimentally as shown in Fig. 8 in which the dashed lines are linear fits performed near the transition threshold (only the first three experimental points were retained).

In the NUP regime, above ρ_2, all modes Θ_n and Φ_n with $n\geq 1$ are time dependent, and the Fourier spectrum of

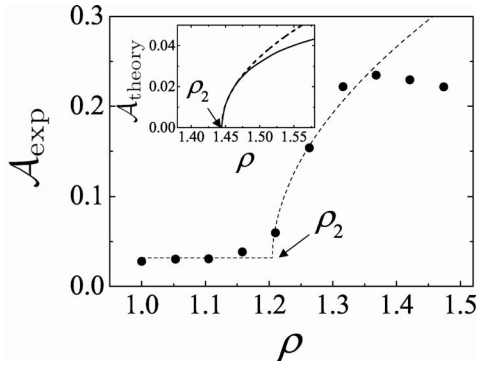

Fig. 7. Scaling law for the amplitude $\mathcal{A}$ of the limit cycle born at the transition UP1→NUP. Experimental data (filled circles) fitted by $(\rho-\rho_2)^\gamma$ near ρ_2, whose best fit gives $\gamma=0.46\pm0.08$. Inset: theory (solid curve) by which the best fit (dashed curve) near ρ_2 gives $\gamma=1/2$.

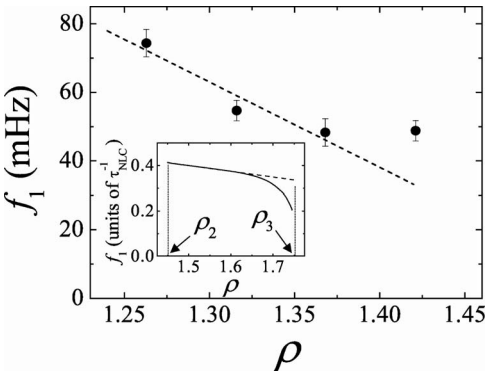

Fig. 8. Scaling law for the frequency of the limit cycle born through the transition UP1→NUP. Experiment (filled circles) with linear fit near the bifurcation threshold (dashed line). Inset: theory (solid curve) with linear fit near ρ_2 (dashed line).

their oscillating part contains frequencies mf_1, where m is an integer. The spectra ($\mathcal{S}$) of the phase delay Δ, the director components $n_{x,y}$, and the output intensities $I_{x,y}$ have peaks at frequencies given by simple formulas, in agreement with preceding experimental and theoretical research reported independently in Refs. 20 and 35:

$$\mathcal{S}(\Delta) = \{mf_1\},$$

$$\mathcal{S}(n_{x,y}) = \{f_0, mf_1 \pm f_0\},$$

$$\mathcal{S}(I_{x,y}) = \{2f_0, mf_1 \pm 2f_0\}. \quad (6)$$

The nature of the spectra obviously depends on the incident intensity. The spectral analysis of both the experimental and the corresponding theoretical results reveals that the relative weight of the higher harmonics increase with ρ and that the amplitude of a given harmonic decays rapidly with increasing m.

As ρ approaches ρ_3, the NUP limit cycle eventually collides with the unstable UPS branch, the UP2 regime being the final state (see Fig. 2). The situation is summarized in Fig. 9, which shows the nutation motion in the reconstructed phase space $X(t+\tau_d)$ versus $X(t)$, where $X = I_{\text{center}}/\rho$ and τ_d is a time delay, for the UP1, NUP, and UP2 regimes. In the reconstructed space, the UP states are represented by a fixed point (I_{center} is constant), whereas a NUP state is represented by a limit cycle. We identify next the transition NUP→UP2 as a homoclinic bifurcation.

C. Homoclinic Bifurcation

The stability analysis of the UPS branch reveals that the relevant eigenvalue $\lambda_{\max}$, which belongs to the UPS branch at $\rho=\rho_3$, is real and positive. Moreover, starting near the UPS solution, the final state can be either a NUP limit cycle or a UP2 limit cycle, depending on the chosen initial conditions. In fact, the unstable UPS branch represents the saddle separatrix that divides the regions of attraction of the NUP state (or, below ρ_2, the UP1 state) from that of the largely reoriented UP2 state. When the NUP limit circle approaches the UPS branch, the nutation period $1/f_1$ correspondingly increases (Fig. 8). More precisely, this period appears to diverge logarithmically at $\rho_3 \approx 1.75$, as shown in Fig. 10. Indeed, with a parameterization of the divergence with the function $a+b\ln(\rho_3-\rho)$, perfect agreement (solid curve) with the calculated values (filled circles) is obtained for $a \simeq 1.249$ and $b \simeq -0.612$. This particular nature of the singularity at $\rho=\rho_3$ guarantees that the discontinuous transition NUP→UP2 (see Fig. 2) has the character of a homoclinic bifurcation.[21–23] In fact, we deal here with a homoclinic bifurcation of the simplest type in which a limit cycle collides with a saddle point having only one unstable direction (all the eigenvalues have a negative real part except one, which is real and positive). The present identification confirms and extends a preliminary account[35] of this bifurcation.

As ρ approaches the homoclinic bifurcation point, the trajectory of the director approaches the unstable UPS orbit for longer and longer intervals. This is demonstrated in Fig. 11 where the director trajectory is plotted in the planes (n_x, n_y) and $(n_x^{\text{rot}}, n_y^{\text{rot}})$ for ρ close to ρ_3. In the f_0(NUP)-rotating frame, the UPS branch is still a circle [Fig. 11(b)] because, for a given ρ below ρ_3, f_0(NUP) is approaching f_0(UPS) from above [see Fig. 5(b)]. The system evolves near the unstable UPS limit cycle, represented by the dashed curve (see Figs. 2 and 11). The dynamics near ρ_3 possesses two time scales, a slow one and a fast one, as expected from the homoclinic nature of the transition. Figure 12 emphasizes this point, in which the phase shift $\Delta(t)$ and the instantaneous angular velocity $\Omega(t) = d\Phi_0/dt$ are plotted versus time. When $\Delta \simeq 2\pi$, the angular velocity has some constant value, more than 1 order of magnitude smaller than the value reached when $\Delta \simeq \pi$. Recalling that the total angular momentum transferred to the NLC by a photon is $(1-\cos\Delta)\hbar$, one can interpret the slow regime as a situation in which there is almost no net angular-momentum transfer, whereas the fast regime corresponds to quasi-optimal angular-momentum transfer.

At $\rho=\rho_3$ the system jumps to a new state of UP of the director (UP2) with a large reorientation ($\Theta \simeq 74°$) and slow precession rate. As displayed in Fig. 2, starting from

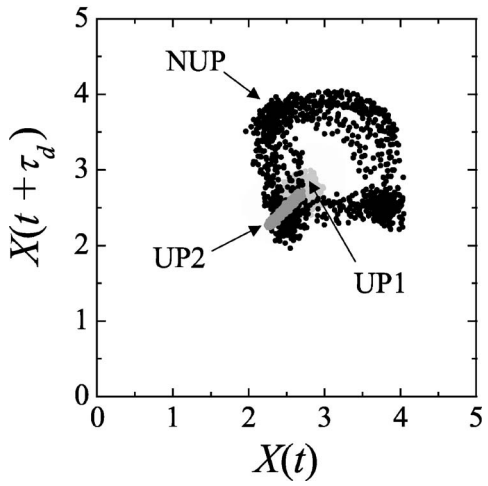

Fig. 9. Reconstructed experimental nutation phase space $X(t+\tau_d)$ versus $X(t)$, where $X=I_{\text{center}}/\rho$ and τ_d is a time delay. Light gray dots, the UP1 state between the OFT and the secondary Hopf instability [$\rho \sim (1+\rho_2)/2$]; black dots, the NUP state between the Hopf and the homoclinic bifurcation [$\rho \sim (\rho_2+\rho_3)/2$]; and dark gray dots, the UP2 state just above the homoclinic bifurcation at $\rho=\rho_3$. The time delay is $\tau_d = 6s$.

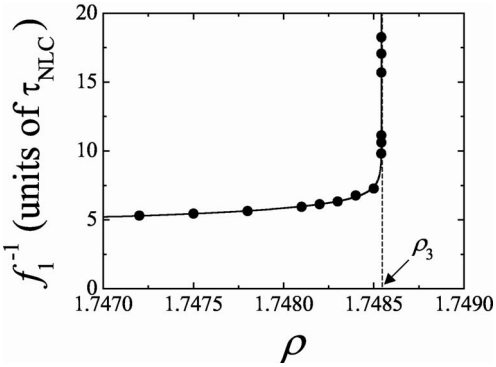

Fig. 10. Characterization of the homoclinic bifurcation $f_1^{-1}(\rho) = \mathcal{O}[\ln(\rho_3 - \rho)]$ near ρ_3. The solid curve is the best fit to the theoretically calculated values (filled circles).

the stable UP2 branch above ρ_3 and lowering the excitation intensity, one finds a large and rather complicated hysteretic cycle, which eventually flips back to the UP1 solution at $\rho_3^* = 1.09$. This part of the UP2 branch consists of alternatively stable and unstable regions exhibiting a series of saddle-node bifurcations. This result was already obtained in the framework of an approximate model[15]; however, experimental evidence of such multistability has yet to be observed.

D. Discussion

One can make an instructive comparison of our results with those of another well-studied geometry, namely, that of a light wave with ordinary linear polarization at oblique incidence (OLPO) (typically, 2°–8°). The dynamics is quite rich in this case, too, and, although the symmetries of the two systems are different, one has an analogous sequence of transitions, namely, an OFT, then a secondary, supercritical Hopf bifurcation, followed by a homoclinic bifurcation (see Refs. 6–8 for a theoretical description and Ref. 36 for a recent experimental study). In both cases, the competition between symmetric and asymmetric reorientation modes has been demonstrated to be at the origin of the secondary instability.[18,37]

In the OLPO geometry, one has in the unperturbed state one reflection symmetry, which in the OFT is broken spontaneously, yielding two equivalent fixed points that subsequently undergo the Hopf bifurcation. The resulting limit cycles are characterized by a single frequency. In the circular polarization (CP) case, on the other hand, one has at outset isotropy but no reflection symmetry (chirality is broken). The spontaneous breaking of this symmetry in the OFT yields the uniformly precessing UP1 state. Because this state is periodic in time (frequency f_0), the subsequent Hopf bifurcation yields a quasi-periodic state characterized by the two frequencies f_0 and f_1. From the symmetry properties, it follows that there are no higher harmonics in f_0 or, equivalently, in the frame rotating uniformly with frequency f_0 the system performs a simple limit cycle with frequency f_1.

When approaching the homoclinic bifurcation, the periodic or quasi-periodic orbits collide with saddles, which are of quite different character in the two systems. In the OLPO case it is the unperturbed state $\mathbf{n} = (0,0,1)$, which is here an unstable fixed point. Clearly then, the homoclinic bifurcation can mediate gluing of the two symmetry-equivalent orbits. In the CP geometry the saddle corresponds to an unstable periodic state (UPS) that lies outside the quasi-periodic orbit and mediates a discontinuous transition to a largely distorted state.

A further (experimental) difference is that it is more difficult to observe the homoclinic trajectory in the CP than in the OLPO case. The presence of unavoidable orientational fluctuations that initiate the irreversible transition NUP→ UP2 [see Fig. 2(a)] make long-time observation of this regime in the CP case difficult.

Finally we should mention that in an experimental setting, the incident beam is often tightly focused, giving rise to an angular spread $\Delta\theta = \lambda/\pi w_0$ (w_0 = beam waist) that may not always be negligible. Under the present experimental conditions, we estimate that $\Delta\theta \simeq 0.6°$, which safely rules out substantial effects due to nonzero angle of incidence.

4. CONCLUSION

In this paper we have studied the reorientation dynamics of a homeotropically aligned nematic liquid-crystal film excited by circularly polarized light at normal incidence. Our theoretical model for the director's dynamics has allowed a complete determination of the bifurcation scenario. Our main results can be summarized as follows.

First, we have shown that the secondary instability above the primary optical Fréedericksz transition threshold is a supercritical Hopf bifurcation. As a result of this bifurcation, a quasi-periodic dynamics is generated in which the motion of the director is a combination of precession and nutation with distinct fundamental frequencies. Second, the discontinuous transition from the quasi-periodic regime to a uniform precession regime has been identified as a homoclinic bifurcation. When possible, the theoretical predictions have been validated experimentally with the help of a pair of observables distinguishing nutation from precession. Third, it would appear that an interpretation of the behavior of the light-induced dynamics based on the transfer of the angular momentum of the light to the LC is a useful guide to extract the underlying physical mechanisms. Finally, we have discussed the analogies and the differences between the present interaction geometry and the case in which the excitation light is an ordinary wave illuminating the LC film at small oblique incidence.

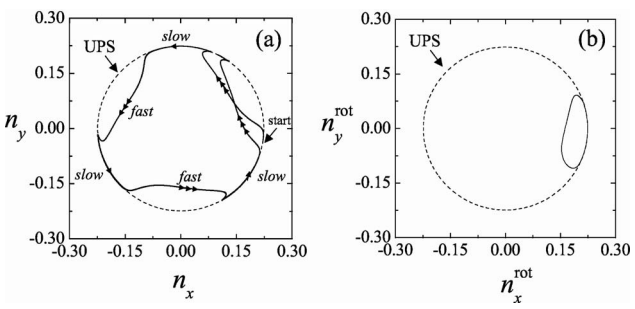

Fig. 11. Homoclinic trajectory in (a) the laboratory frame (n_x, n_y) and (b) the f_0-rotating frame (n_x^{rot}, n_y^{rot}) just below $\rho = \rho_3 (\rho = 1.748542389055)$.

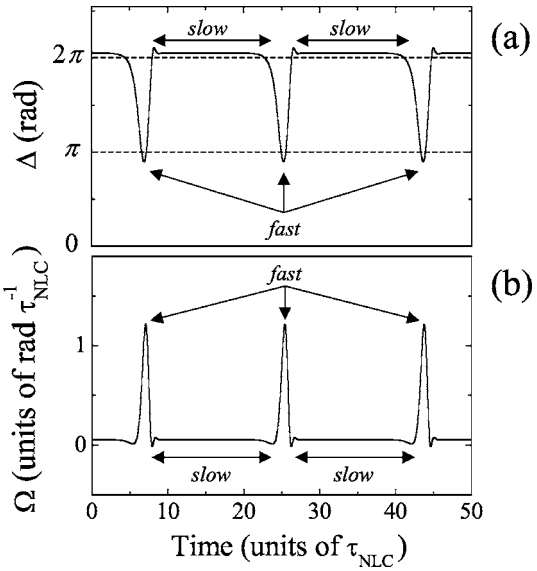

Fig. 12. Calculated dynamics just below $\rho=\rho_3$ ($\rho=1.748542389055$). (a) Phase shift $\Delta(t)$. (b) Instantaneous angular velocity $\Omega(t)=d\Phi_0/dt$.

As mentioned in Section 1, improvements to the theory should involve a generalization to a finite beam size and the inclusion of the flow field excited by the motion of the director. Whereas the latter effect has been taken into account in the description of electric- and magnetic-field-driven instabilities (backflow[38]), it has apparently never been considered, until quite recently, in the context of light-driven dynamical phenomena. The first exploratory backflow calculations indicate that, in the system considered here, nothing dramatic happens and only small shifts of the positions of the various transitions arise.[39] A further refinement could also be the inclusion of the lateral spatial degrees of freedom, as first performed in the context of the oblique-incidence instability.[40] To approach such a situation experimentally, one needs, however, a large-aspect-ratio laser beam. This can probably be achieved, without increasing the power output of the laser, by using an appropriate dye-doped LC mixture that is known to reduce the Fréedericksz threshold.[41]

Finally, one could consider what happens to the dynamics when the system is no longer invariant under rotation about the z axis. This situation can be realized by using an elliptically polarized excitation light beam instead of a circular one. The studies on this geometry are few and far apart, and the pioneering (theoretical and experimental) contributions can be found in Refs. 28 and 29. Important differences have been observed already, but nothing equivalent to the secondary instability found in the circular case has been reported yet. With the present theoretical and experimental tools, we have decided to investigate the situation further to understand the consequences of breaking the initial rotational invariance by using an elliptically polarized excitation. Our findings will be presented in a companion paper[30] in which, among other things, we will demonstrate the existence of unpredicted dynamical regimes.

APPENDIX A

In this appendix the equations of motion of the angles Θ and Φ that describe the director and those governing the propagation of the light in the reoriented NLC are given.

For convenience, let us introduce the following normalized quantities. First, we define the normalized elastic constants $k_1=K_1/K_3$ and $k_2=K_2/K_3$, where K_1, K_2, and K_3 are, respectively, the splay, twist, and bend elastic constants of the NLC.[12] Second, the length and time are normalized according to $\xi=z/L$ and $\tau=t/\tau_{\mathrm{NLC}}$, respectively, where L is the cell thickness and $\tau_{\mathrm{NLC}}=\gamma_1 L^2/\pi^2 K_3$ is a characteristic reorientation time, with γ_1 as the rotational viscosity.[12] Finally $\rho=I/I_F^{\mathrm{CP}}$ is defined as the normalized incident intensity, with $I_F^{\mathrm{CP}}=2\pi^2 c\varepsilon_{\parallel}K_3/L^2\epsilon_a\sqrt{\epsilon_{\perp}}$ as the threshold intensity (watts per inverse square meter) for the OFT under circularly polarized excitation, where $\epsilon_{\perp}(\epsilon_{\parallel})$ is the dielectric permittivity perpendicular (parallel) to $\mathbf{n}$ and $\epsilon_a=\epsilon_{\parallel}-\epsilon_{\perp}$ is the corresponding anisotropy.

The equations for $\Theta(\xi,\tau)$ and $\Phi(\xi,\tau)$ are obtained from the equations of motion of the director $\mathbf{n}$, which include the elastic, electromagnetic, and viscous torques,[25]

$$\frac{\partial\Theta}{\partial\tau} = [1-(1-k_1)\sin^2\Theta]\frac{1}{\pi^2}\frac{\partial^2\Theta}{\partial\xi^2} - \frac{\sin 2\Theta}{2}\left\{(1-k_1)\times\left(\frac{1}{\pi}\frac{\partial\Theta}{\partial\xi}\right)^2 + [1-2(1-k_2)\sin^2\Theta]\left(\frac{1}{\pi}\frac{\partial\Phi}{\partial\xi}\right)^2 - 2\rho\frac{n_e^4}{n_o^4}|A_e|^2\right\},$$

$$\frac{\partial\Phi}{\partial\tau} = \frac{1}{\pi^2\sin^2\Theta}\frac{\partial}{\partial\xi}\left\{[1-(1-k_2)\sin^2\Theta]\sin^2\Theta\frac{\partial\Phi}{\partial\xi}\right\} + \rho\frac{n_e^2}{n_o^2}[A_eA_o^*\exp[i\psi(\xi,\tau)] + \mathrm{c.c.}]. \quad \text{(A1)}$$

In these equations, the amplitudes A_o, A_e are expressed as functions of the amplitudes of the ordinary (E_o) and extraordinary ($E_e^{\perp}$) electric fields in the (x,y) plane as

$$E_o(\xi,\tau) = A_o(\xi,\tau)\exp(i\kappa_0 n_o\xi),$$

$$E_e^{\perp}(\xi,\tau) = A_e(\xi,\tau)\exp\left[i\kappa_0\int_0^{\xi}n_e(\xi',\tau)\mathrm{d}\xi'\right], \quad \text{(A2)}$$

where $\kappa_0=2\pi L/\lambda$ is the normalized wave vector of the light beam and

$$n_e(\xi,\tau)=\frac{n_o n_E}{(n_E^2\cos^2\Theta+n_o^2\sin^2\Theta)^{1/2}}, \quad \text{(A3)}$$

with $n_o=\epsilon_{\perp}^{1/2}$ and $n_E=\epsilon_{\parallel}^{1/2}$, respectively, as the eigenordinary and eigenextraordinary refractive indices. Under the geometric-optics approximation ($\kappa_0\gg 1$), the equations governing the propagation of the ordinary and extraordinary waves are written as

$$\frac{\partial A_o}{\partial \xi} = -\frac{\partial \Phi}{\partial \xi}\frac{n_c}{n_o}\exp[i\psi(\xi,\tau)]A_e,$$

$$\frac{\partial A_e}{\partial \xi} = -\frac{1}{2n_e}\frac{\partial n_e}{\partial \xi}A_e + \frac{\partial \Phi}{\partial \xi}\frac{n_o}{n_e}\exp[-i\psi(\xi,\tau)]A_o, \quad \text{(A4)}$$

where $\psi(\xi,\tau)$ corresponds to the total phase shift between the e and o waves at the location ξ and time τ if the light propagation would have been adiabatic through the reoriented NLC (i.e., the so-called Mauguin regime), namely,

$$\psi(\xi,\tau) = \kappa_0 \int_0^{\xi} [n_e(\xi',\tau) - n_o]\mathrm{d}\xi'. \quad \text{(A5)}$$

The total phase shift Δ defined by Eq. (4) is thus

$$\Delta(\tau) = \psi(1,\tau). \quad \text{(A6)}$$

Finally, the evolution equations for the amplitudes $\Theta_n(\tau)$ and $\Phi_n(\tau)$ are obtained by projecting Eqs. (A1) on each mode [Eqs. (1) and (2)], leading to a set of coupled equations given by

$$\frac{\mathrm{d}\Theta_n}{\mathrm{d}\tau} = 2\int_0^1 \frac{\partial \Theta}{\partial \tau}\sin(n\pi\xi)\mathrm{d}\xi,$$

$$\frac{\mathrm{d}\Phi_n}{\mathrm{d}\tau} = 2\int_0^1 \frac{\partial \Phi}{\partial \tau}\sin[(n+1)\pi\xi]\sin(\pi\xi)\mathrm{d}\xi. \quad \text{(A7)}$$

Equations (A7) are then solved simultaneously with those for the optical fields [Eqs. (A4)] under appropriate boundary conditions. For the angles Θ and Φ, the strong anchoring conditions

$$\Theta(0,\tau) = \Theta(1,\tau) = 0,$$

$$\frac{\partial \Phi}{\partial \xi}(0,\tau) = \frac{\partial \Phi}{\partial \xi}(1,\tau) = 0 \quad \text{(A8)}$$

are explicitly satisfied with the modal expansion [Eqs. (1) and (2)], leaving the choice of initial values for $\Theta_n(0)$ and $\Phi_n(0)$ (almost) arbitrary. In practice, one integrates away (in time) from the initial conditions and starts to record the results as soon as the solutions have reached stationarity.

For the electric field amplitudes, the boundary conditions are given by the polarization of the incident excitation light. Without loss of generality, we may choose the x axis along the major axis of the polarization ellipse of the incident light. In this case the amplitudes A_o, A_e at $\xi=0$ (normalized to the incident electric field amplitude) are given at time τ by

$$|A_o(0,\tau)|^2 = \tfrac{1}{2}\{1 - \cos[2\Phi(0,\tau)]\cos 2\chi\},$$

$$|A_e(0,\tau)|^2 = \tfrac{1}{2}\{1 + \cos[2\Phi(0,\tau)]\cos 2\chi\},$$

$$A_e(0,\tau)A_o(0,\tau)^* = -\tfrac{1}{2}\{\sin[2\Phi(0,\tau)]\cos 2\chi + i\sin 2\chi\}, \quad \text{(A9)}$$

where the ellipticity angle $\chi(-\pi/4 \leqslant \chi \leqslant \pi/4)$ is related to the ratio between the minor (b) and the major (a) axes of the polarization ellipse by $\tan\chi = \pm b/a$.[42] The case $\chi=0$ ($\chi = \pm\pi/4$) corresponds to a linearly (circularly) polarized excitation beam, and intermediate values refer to elliptical polarization. Because the sign of χ determines the handedness of the polarization and hence the sense of rotation of the director around the z axis, it is sufficient to consider only positive values of χ. In the case of a circularly polarized light, the Φ (and thus the τ) dependence disappears from the boundary conditions (A9), which simplify to

$$|A_e(0,\tau)|^2 = |A_o(0,\tau)|^2 = \tfrac{1}{2},$$

$$A_e(0,\tau)A_o(0,\tau)^* = -\frac{i}{2}. \quad \text{(A10)}$$

We thank G. Demeter for stimulating discussions and help during the course of this study. E. Brasselet, T. V. Galstian, and L. J. Dubé acknowledge financial support from the National Science and Engineering Research Canada. E. Brasselet, D. O. Krimer, and L. Kramer acknowledge financial support from the Deutsche Forschungsgemeinschaft under Kr 690/16, 436UNG113/151/1. Financial support from the European Graduate School, Non-Equilibrium Phenomena and Phase Transitions in Complex Systems is also gratefully acknowledged.

E. Brasselet, the corresponding author, can be reached by e-mail at ebrassel@ens-lyon.fr. D. O. Krimer's e-mail address is Dmitry.Krimer@uni-bayreuth.de.

*Also at Centre d'Optique, Photonique, et Laser, Université Laval, Québec, Canada G1K7P4.

†Also at Laboratoire de Chime-Physique Matière et Rayonnement, Université Pierre et Marie Curie, 75231 Paris 05, France.

‡Lorenz Kramer passed away on April 5, 2005.

REFERENCES AND NOTES

1. N. V. Tabiryan, A. V. Sukhov, and B. Y. Zel'dovich, "Orientational optical nonlinearity of liquid-crystals," Mol. Cryst. Liq. Cryst. **136**, 1–139 (1986).
2. I. C. Khoo and S. T. Wu, *Optics and Nonlinear Optics of Liquid Crystals* (World Scientific, 1993).
3. E. Santamato, "Giant optical nonlinearities in nematic liquid crystals," in *Nonlinear Optical Material and Devices for Applications in Information Technology*, A. Miller, K. R. Welford, and B. Daino, eds. (Kluwer Academic, 1995), pp. 103–139.
4. F. Simoni, *Nonlinear Optical Properties of Liquid Crystals and Polymer Dispersed Liquid Crystals* (World Scientific, 1997).
5. G. Cipparrone, V. Carbone, C. Versace, C. Umeton, R. Bartolino, and F. Simoni, "Optically induced chaotic behavior in nematic liquid-crystal films," Phys. Rev. E **47**, 3741–3744 (1993).
6. G. Demeter and L. Kramer, "Transition to chaos via gluing bifurcations in optically excited nematic liquid crystals," Phys. Rev. Lett. **83**, 4744–4747 (1999).
7. G. Demeter, "Complex nonlinear behavior in optically excited nematic liquid crystals," Phys. Rev. E **61**, 6678–6688 (2000).
8. G. Demeter and L. Kramer, "Numerical investigation of

optically induced director oscillations in nematic liquid crystals," Phys. Rev. E **64**, 020701 (R) (2001).
9. E. Brasselet, "Comment on 'Numerical investigation of optically induced director oscillations in nematic liquid crystals'," Phys. Rev. E (to be published).
10. B. Piccirillo, C. Toscano, F. Vetrano, and E. Santamato, "Orbital and spin photon angular momentum transfer in liquid crystals," Phys. Rev. Lett. **86**, 2285–2288 (2001).
11. A. Vella, A. Setaro, B. Piccirillo, and E. Santamato, "On–off intermittency in chaotic rotation induced in liquid crystals by competition between spin and orbital angular momentum of light," Phys. Rev. E **67**, 051704 (2003).
12. P. G. de Gennes and J. Prost, *The Physics of Liquid Crystals*, 2nd ed. (Clarendon, 1993).
13. A. S. Zolot'ko, V. F. Kitaeva, N. Kroo, N. N. Sobolev, and L. Csillag, "Light-induced Fréedericksz transition in an MBBA crystal," Pis'ma Zh. Eksp. Teor. Fiz. **34**, 263–267 (1981) [JETP Lett. **34**, 250–254 (1981)].
14. E. Santamato, B. Daino, M. Romagnoli, M. Settembre, and Y. R. Shen, "Collective rotation of molecules driven by the angular momentum of light in a nematic film," Phys. Rev. Lett. **57**, 2423–2426 (1986).
15. A. S. Zolot'ko and A. P. Sukhorukov, "Fréedericksz transition induced in nematic liquid-crystal by circularly polarized-light wave," Pis'ma Zh. Eksp. Teor. Fiz. **52**, 707–710 (1990) [JETP Lett. **52**, 62–65 (1990)].
16. L. Marrucci, G. Abbate, S. Ferraiuolo, P. Maddalena, and E. Santamato, "Self-stimulated light scattering in nematic liquid crystals: theory and experiment," Phys. Rev. A **46**, 4859–4868 (1992).
17. E. Brasselet and T. V. Galstian, "Optical control of molecular orientational dynamics in liquid crystals," Opt. Commun. **186**, 291–302 (2000).
18. E. Brasselet, B. Doyon, T. V. Galstian, and L. J. Dubé, "New laser induced spatio-temporal transition in nematics," Phys. Lett. A **299**, 212–216 (2002).
19. E. Brasselet, B. Doyon, T. V. Galstian, and L. J. Dubé, "Optically induced dynamics in nematic liquid crystals: the role of twist deformation and asymmetry," Phys. Rev. E **67**, 031706 (2003).
20. E. Brasselet, B. Doyon, T. V. Galstian, and L. J. Dubé, "Optically induced dynamics in nematic liquid crystals: The role of finite beam size," Phys. Rev. E **69**, 021701 (2004).
21. For a classification of the different types of bifurcation, the reader is invited to consult J. Guckenheimer and P. Holmes, *Nonlinear Oscillations, Dynamical Systems, and Bifurcation of Vector Fields* (Springer-Verlag, 1983). See also Refs. 22 and 23.
22. J. Hale and H. Koçak, *Dynamics and Bifurcations* (Springer-Verlag, 1991).
23. P. Glendinning, *Stability, Instability and Chaos* (Cambridge U. Press, 1996).
24. M. Abramowitz and I. A. Stegun, *Handbook of Mathematical Functions* (Dover, 1970).
25. B. Y. Zel'dovich and N. Tabiryan, "Theory of optically induced Fréedericksz transition," Zh. Eksp. Teor. Fiz. **82**, 1126–1146 (1982) [Sov. Phys. JETP **55**, 656–666 (1982)].
26. From Merck datasheets. The refractive indices are measured at 20°C and $\lambda = 589$ nm.
27. G. Cipparrone, D. Duca, C. Versace, C. Umeton, and N. V. Tabiryan, "Direct optical measurements of the ratio K_3/γ_1 in nematic liquid crystals," Mol. Cryst. Liq. Cryst. Sci. Technol., Sect. A **266**, 263–268 (1995).
28. E. Santamato, G. Abbate, P. Maddalena, L. Marrucci, and Y. R. Shen, "Laser-induced nonlinear dynamics in a nematic liquid-crystal film," Phys. Rev. Lett. **64**, 1377–1380 (1990).
29. A. Vella, B. Piccirillo, and E. Santamato, "Coupled-mode approach to the nonlinear dynamics induced by an elliptically polarized laser field in liquid crystals at normal incidence," Phys. Rev. E **65**, 031706 (2002).
30. D. O. Krimer, L. Kramer, E. Brasselet, T. V. Galstian, and L. J. Dubé, "Bifurcation analysis of optically induced dynamics in nematic liquid crystals: elliptical polarization at normal incidence," J. Opt. Soc. Am. B **22**, 1681–1690 (2005).
31. S. D. Durbin, S. M. Arakelian, and Y. R. Shen, "Laser-induced diffraction rings from a nematic-liquid-crystal film," Opt. Lett. **6**, 411–413 (1981).
32. From the weakly nonlinear stability analysis, we find that the nature of the OFT is governed by the sign of the coefficient $C = k_1 - (9/4)(\epsilon_a/\epsilon_\parallel)$. $C < 0$ corresponds to a subcritical OFT (i.e., first order), whereas $C > 0$ corresponds to a supercritical OFT (i.e., second order). Incidentally, this criterion is identical to the one derived by Ong in the case of OFT under linearly polarized light.[33] With the present parameters, $C = 0.154$ and the OFT is actually supercritical. However, the solution branch turns over and becomes subcritical (and unstable) already at $\rho = 1 + \delta\rho$ where $\delta\rho \simeq 10^{-6}$. This explains why the OFT appears to be subcritical on the scale used in Fig. 2. In fact, although $\delta\rho$ increases when the cell thickness is decreased, even at $L = 10$ μm, the subcritical region is still too small ($\delta\rho \simeq 10^{-4}$) to be observed experimentally.
33. H. L. Ong, "Optically induced Fréedericksz transition and bistability in a nematic liquid crystal," Phys. Rev. A **28**, 2393–2407 (1983).
34. I. C. Khoo, T. H. Liu, and P. Y. Yan, "Nonlocal radial dependence of laser-induced molecular reorientation in a namatic liquid crystal: theory and experiment," J. Opt. Soc. Am. B **4**, 115–120 (1987).
35. D. O. Krimer, G. Demeter, and L. Kramer, "Orientational dynamics induced by circularly polarized light in nematic liquid crystals," Mol. Cryst. Liq. Cryst. **421**, 117–131 (2004).
36. V. Carbone, G. Cipparrone, and G. Russo, "Homoclinic gluing bifurcations during the light induced reorientation in nematic-liquid-crystal films," Phys. Rev. E **63**, 051701 (2001).
37. N. V. Tabiryan, A. L. Tabiryan-Murazyan, V. Carbone, G. Cipparrone, C. Umeton, C. Versace, and T. Tschudi, "Temporal instability due to competing spatial patterns in liquid crystals in the light field," Opt. Commun. **154**, 70–74 (1998).
38. For some recent research, see S. A. Jewell and J. R. Sambles, "Observation of backflow in the switch-on dynamics of hybrid aligned nematic," Appl. Phys. Lett. **84**, 46–48 (2004).
39. D. O. Krimer, G. Demeter, and L. Kramer, "Influence of the backflow effect on the orientational dynamics induced by light in nematics," Phys. Rev. E **71**, 051711 (2005).
40. D. O. Krimer, G. Demeter, and L. Kramer, "Pattern-forming instability induced by light in pure and dye-doped nematic liquid crystals," Phys. Rev. E **66**, 031707 (2002).
41. I. Jánossy, A. D. Lloyd, and B. S. Wherrett, "Anomalous optical Fréedericksz transition in an absorbing liquid crystal," Mol. Cryst. Liq. Cryst. **179**, 1–12 (1990).
42. C. Brosseau, *Fundamentals of Polarized Light: a Statistical Optics Approach* (Wiley, 1998).